Spatio-temporal dynamics of summer flounder (*Paralichthys dentatus*) on the Northeast US Shelf

Charles T. Perretti[1]*, James T. Thorson[2]
[1]Northeast Fisheries Science Center, National Marine Fisheries Service (NMFS), 166 Water Street, Woods Hole, MA 02543, USA,
[2]Habitat and Ecosystem Process Research Program, Alaska Fisheries Science Center, NMFS, 7600 Sand Point Way N.E., Seattle, WA 98115, USA

Abstract

Summer flounder (*Paralichthys dentatus)* are an economically and ecologically important fish on the Northeast U.S. shelf. There is evidence that their spatial distribution has shifted over time. However, there are conflicting reports on the importance of various potential drivers of the shift. Here, we investigate whether the stock has shifted and the extent to which this can be attributed to changes in abundance, size-structure, environmental variables, and fishing. We do so using a vector-autoregressive spatio-temporal model that incorporates data from two seasonal bottom trawl surveys that together span the nearshore and offshore Northeast US shelf over the past 41 years. We find that the summer flounder distribution has shifted north and east in both the spring and fall. The shift is observed in both recruits and spawners, with recruits shifting northward faster than spawners, suggesting that increased spawner abundance may not be driving the shift in recruits. We find that only a small portion of the variability in distribution can be attributed to changes in abundance, fishing, or environmental covariates. Instead, the shift is most strongly attributed to unidentified factors.

*To whom correspondence should be addressed
Email: charles.perretti@noaa.gov
Running title: Spatio-temporal distribution of summer flounder

1. Introduction

Summer flounder (*Paralichthys dentatus*) support a valuable flatfish fishery on the Northeast US shelf (NE Shelf) with combined recreational and commercial landings exceeding 4,000 metric tons in 2017 (NEFSC, In Review). The population spans from North Carolina to Maine and undergoes annual migrations from the edge of the continental shelf in the winter to nearshore habitat in the fall (Terceiro, 2001; Sackett et al., 2007). There is evidence that the population and the fishery has shifted north in recent years (Nye et al., 2009; Pinsky and Fogarty, 2012), although the driver of this shift is not agreed upon.

Summer flounder are one of many species on the NE Shelf that appear to be shifting northward. There is increasing evidence for poleward shifts in marine fishes globally (Perry et al., 2005; Pinsky et al., 2013), and on the NE shelf, these shifts have been linked to environmental variables, fishing (Adams et al., 2018), and population structure (Bell et al., 2015). Studies of summer flounder have yielded conflicting conclusions as to the relative importance of these drivers. Of studies primarily focused on environmental drivers, some have highlighted local drivers such as tow bottom temperature and salinity (Pinsky et al., 2013; Kleisner et al., 2017), others have identified regional drivers such as summer duration on the NE Shelf (Henderson et al., 2017), while others have highlighted basin-scale drivers such as the Atlantic Multidecadal Oscillation (Nye et al., 2009). Studies including fishing as an explanatory variable concluded that fishing-induced changes in population abundance and size-structure are most important (Bell et al., 2014, 2015). While it is possible that all of these factors are at play, the relative importance of each remains unresolved.

Importantly, most previous studies of distribution shifts in summer flounder have estimated the importance of the spatial driver outside of a spatial model itself. Typically a sample-based calculation is performed on spatial data that condenses each year of data into a single estimate of center-of-gravity (e.g., using a design-based estimator; Woillez et al., 2007). Center-of-gravity estimates are then regressed against a suite of potential drivers to determine significance. As has been noted elsewhere (Thorson et al., 2017), this approach does not quantify the amount of variation in the observations attributed to the driver, which is often of interest to both ecologists and managers.

In contrast, we use a vector auto-regressive spatio-temporal model (VAST) that incorporates potential explanatory variables directly into the spatial model, thus providing an estimate of the variance in the spatial distribution attributed to potential driving variables. We use data from two seasonal bottom trawl surveys, which together span the nearshore and offshore habitat of summer flounder over the past 41 years. We quantify the extent to which summer flounder have shifted poleward, and then examine whether the shift can be attributed to changes in environmental variables, fishing, population abundance, size-structure or some other unidentified source.

2. Methods

2.1 Biomass data

We include two bi-annual bottom trawl datasets that together span the nearshore and offshore summer flounder habitat: (1) NMFS, and (2) NEAMAP (Fig.1). The surveys occur in the spring and fall, with the NEAMAP survey starting in the fall of 2007. We fit the VAST model to each season separately to provide two estimates of change in distribution. The NMFS survey spans North Carolina to Maine and since 2009 primarily samples waters greater than 3 miles from shore. The NEAMAP survey samples nearshore waters from North Carolina to Rhode Island.

The NMFS survey gear, sampling procedures and design details are described in Azarovitz (1981) and Smith (2002). The full nearshore strata set began consistent sampling in 1976; therefore we include data from 1976 to 2016 (41 years with two surveys per year). We used vessel-standardized catchability and selectivity coefficients from previous paired-tow vessel calibration studies (Miller, 2013; Miller et al., 2010) to account for vessel changes within the NMFS survey.

To explore spatial differences across size-classes we divide individuals into two size categories roughly corresponding to recruits and spawners. We define recruits as individuals less than or equal to 30cm, and spawners as those greater than 30cm, which roughly corresponds to length at age-1. The length-weight relationship of summer flounder has been relatively constant over time (NEFSC, In Review), therefore individual lengths were converted to biomass using the length–weight relationship for summer flounder from Wigley et al. (2003).

2.2 Model structure

We model the probability of observing a catch *c* of summer flounder as the product of the probability of encountering summer flounder and the probability of a particular biomass of summer flounder given an encounter (i.e., a delta-model). This two-part model combines the process governing occupancy and the process governing biomass conditional on occupancy.

$$\Pr[c] = \Pr[C > 0] \times \Pr[C = c|C > 0] \tag{1}$$

where $c$is the catch of sample i, $\Pr[C > 0]$ is the probability of a positive catch (and inversely, $1 - \Pr[C > 0]$ is the probability of a zero catch), and $\Pr[C = c|C > 0]$ is the probability of catch *c* given that the catch is positive. $\Pr[C > 0]$ is modeled as a Bernoulli random variable, and $\Pr[C = c|C > 0]$ is modeled as a Gamma distributed random variable.

$$\Pr[C > 0] = p_i \tag{2}$$

$$\Pr[C = c|C > 0] = Gamma(c, \sigma^{-2}, \lambda_i\sigma^2) \tag{3}$$

where $\sigma^{-2}$and $\lambda_i\sigma^2$ are the shape and scale terms of the Gamma distribution, respectively, making $\lambda_i$the expected value of sample *i*. Both p_i and λ_i are modeled as generalized linear mixed models.

$$logit(p_i) = \;_p(t_i, c_i) + \omega_p(s_i, c_i) + \epsilon_p(s_i, c_i, t_i) + \sum_{j=1}^{j} \alpha_p(j, c_i)x(j, s_i, t_i) + \;_p q_i \tag{4}$$

$$log(\lambda_i) = \;_\lambda(t_i, c_i) + \omega_\lambda(s_i, c_i) + \epsilon_\lambda(s_i, c_i, t_i) + \sum_{j=1}^{j} \alpha_\lambda(j, c_i,)x(j, s_i, t_i) + \;_\lambda q_i \tag{5}$$

where $\;_p(t_i, c_i)$ is the intercept of the probability of occurrence for year *t* and length-group *c* and is modeled as a random walk, $\omega_p(s_i, c_i)$ is a time-invariant unexplained spatial effect for knot *s* and length-group *c*, and $\epsilon_p(s_i, c_i, t_i)$ is a time-varying unexplained spatial effect for knot *s* and length-group *c* in year *t* (i.e., an interaction of spatial variation and year). $\alpha_p(j, c_i)$ is the effect of covariate *j* on length-group *c*, where n_j is the number of covariates, and $x(j, s_i, t_i)$ is the value of covariate *j* in knot *s* in year *t*. $\;_p$ is a calibration effect converting NEAMAP units to NMFS units (i.e., a statistical vessel calibration), and q_i is an indicator variable for NEAMAP units. Both p_i and λ_i must be positive, and p_i must be bounded within

[0,1]. Therefore a logit-link is used for p_i and a log-link is used for λ_i. Parameters are defined identically for the expected biomass given occurrence model of $\log(\lambda_i)$.

The spatial processes $\omega_p(s_i, c_i)$ and $\omega_\lambda(s_i, c_i)$ are modeled as Gaussian Markov random fields with correlations over two spatial dimensions and among length bins.

$$vec(\boldsymbol{\Omega}_\lambda) \sim GRF(0, \boldsymbol{R}_\lambda \otimes \boldsymbol{V}_{\omega\lambda}) \tag{6}$$

where $\boldsymbol{\Omega}_\lambda$ is a matrix composed of $\omega_\lambda(s, c)$ at every knot s and length bin c, $\boldsymbol{R}_\lambda$ is the correlation among knots, and $\boldsymbol{V}_{\omega\lambda}$ is the correlation among length bins

$$\boldsymbol{V}_{\omega\lambda} = \boldsymbol{L}_{\omega\lambda}\boldsymbol{L}_{\omega\lambda}^T \tag{7}$$

where $\boldsymbol{L}_{\omega\lambda}$ is a loadings matrix representing covariance among length bins.

Spatial covariance between knots s and s^* is modeled as a Matern process

$$\boldsymbol{R}_\lambda(s, s^*) = \frac{1}{2^{\upsilon-1}\Gamma(\upsilon)}(\kappa_\lambda \boldsymbol{H}|s - s^*|)^\upsilon K_\upsilon(\kappa_\lambda \boldsymbol{H}|s - s^*|) \tag{8}$$

where υ is a smoothness parameter that is fixed at 1.0, κ_λ controls the distance over which correlation declines to zero, K_υ is a Bessel function, and $\boldsymbol{H}$ is a two-dimensional anisotropic distance function. The spatio-temporal processes $\epsilon_p(s_i, c_i, t_i)$ and $\epsilon_\lambda(s_i, c_i, t_i)$ are fit independently to each year and are also modeled as Gaussian Markov random fields with Matern covariance. For further details on the VAST model structure see Thorson and Barnett (2017) and references therein. Parameter estimation was performed in Template Model Builder (Kristensen et al., 2016) in the *R* statistical computing language. Model convergence was checked by ensuring that the absolute value of the final gradient of the log-likelihood function at the maximum likelihood estimate was less than 0.0001 for all parameters, and that the Hessian of the likelihood function was positive definite.

2.3 Derived quantities

The expected biomass in a knot is the expected density in that knot multiplied by the area associated with that knot.

$$\begin{aligned}\hat{B}_{s,c,t} = a(s) \times\ logit^{-1}&\left({}_p(t,c) + \omega_p(s,c) + \epsilon_p(s,c,t) \right. \\ &\left. + \sum_{j=1}^{n_j} \alpha_p(j,c)x(j,s,t) \right) \\ &\times \exp\left({}_\lambda(t,c) + \omega_\lambda(s,c) + \epsilon_\lambda(s,c,t) + \sum_{k=1}^{n_k} \alpha_\lambda(k,c)x(k,s,t) \right)\end{aligned} \tag{9}$$

where *a(s)* is the area of knot s and $\hat{B}_{s,c,t}$ is the expected biomass in knot s for size-category c in year t. The total biomass of size-category c in year t is then

$$\hat{B}_{c,t} = \sum_{s=1}^{S} \hat{B}_{s,c,t} \tag{10}$$

where n_s is the number of knots. Similarly, the center-of-gravity is

$$\bar{x}_{c,t} = \frac{\sum_{s=1}^{s} \hat{B}_{s,c,t} x_s}{\sum_{s=1}^{n_s} \hat{B}_{s,c,t}} \tag{11}$$

where x_s is the northing or easting value for knot s.

We compare the model-based center-of-gravity to a design-based center-of-gravity where $\hat{B}_{s,c,t}$ is replaced with the mean observed biomass associated with knot s and size-category c, in year t. Only the NMFS dataset was used for this comparison because the design-based estimator is unable to account for vessel effects between the NEAMAP and NMFS survey.

2.4 Covariates

We include both local and regional covariates, where a local covariate varies across space while a regional covariate is a univariate time series representing the covariate over the entire stock area. Specifically, we include local and regional temperature, local depth, regional biomass, and regional fishing pressure. For regional covariates we allow for spatially varying effects by interacting the covariate with the northings of the knot. Local temperature is defined as the average bottom temperature associated with each knot in each year and season, where bottom temperature estimates were obtained following the method of Friedland et al. (*In press*). Linear and quadratic terms were included to allow for a nonlinear response to local temperature. Regional temperature is the annual average shelf-wide temperature for each season using the same data as local temperature. Depth is the average bottom depth of all tows associated with each knot. Regional biomass is the annual stratified mean biomass (kg) per tow from the NEFSC survey in each season, where stratification follows the survey strata scheme (i.e., the conventional design-based estimate of biomass). Regional fishing pressure is defined as the annual recreational and commercial landings of summer flounder divided by regional biomass (relative exploitation). Recreational landings records are not available from 1976 – 1980 therefore we estimated recreational landings as the commercial landings times the ratio of commercial to recreational landings from 1981 – 1989 (a ratio of approximately 0.67). Time series of regional covariates are shown in Fig. 2.

In summary, we include six covariates in each seasonal model:

$$x(s,t) = \left(T_l(s,t), T_l^2(s,t), n(s)T_r(t), D_l(s,t), n(s)B_r(t), n(s)F_r(t)\right)'$$

where $T_l(s,t)$ is the local temperature associated with knot s in year t for a given season, $T_l^2(s,t)$ is similarly defined for temperature-squared, $n(s)$ is the northings of knot s, $T_r(t)$ is regional temperature, $D_l(s,t)$ is the local depth of knot s, $B_r(t)$ is the regional biomass, and $F_r(t)$ is the regional fishing exploitation rate.

In VAST, the spatial random fields ($\omega_p(s,c)$, $\epsilon_p(s,c,t)$, $\omega_\lambda(s,c)$, $\epsilon_\lambda(s,c,t)$) and the covariates can account for changes in distribution over time. The spatial random fields capture residual spatial patterns that cannot be attributed to the fixed effects (e.g., the covariates). Therefore, to examine the relative importance of the covariates versus the spatial random fields we performed a counterfactual analysis in the spirit of Pearl (2009), in which we set the spatial effects in the fitted VAST model to zero and then generate the center-of-gravity time series. The center-of-gravity time series from the model without the random fields was then compared to the time series from the full model to determine the amount of variation that can be attributed to the covariates.

2.5 Biomass trends within geographic subareas

To examine biomass trends in different regions of the NE Shelf, we divide the NE Shelf into north, middle, and south areas that each roughly correspond to one third of the NE Shelf. For each season, the full VAST model was used to predict density within each area using the knots that are located in each area. Total biomass and proportion of biomass is then calculated for each area and plotted. NMFS survey strata associated with each area are listed in Table S1, and boundaries of each area are shown in Fig.3. For each season, the full VAST model is used to predict density within each area using the knots that are located in each area.

3. Results

Model convergence statistics were met for both seasons, and residual plots did not suggest any significant problems with model fit (Figs S1 – S6), although the model tended to under-predict the largest observations. Biomass timeseries show generally low recruitment and reduced spawner biomass in recent years (Fig. 4).

A northward shift in the center-of-gravity was observed, with both size-groups at or near their historical maximum northing in recent years in both seasons (Figs 5 and 6). Results were similar with or without NEAMAP data included in the model (Figs S11–S13). When averaged over both seasons and models, recruits have shifted north approximately 56% faster than spawners (1.4 km/yr for recruits versus 0.9 km/yr for spawners), resulting in recruits shifting approximately 20km further northward than spawners over the entire time series. There has also been an eastward shift in center-of-gravity in both size-groups and seasons, with recent years at or near their historical maximum easterly (Figs 5 and 6). Center-of-gravity times series from the VAST model were similar to that of the design-based estimate (Figs S10 and S11), the main difference being reduced variability in the VAST model (a result also observed elsewhere; Thorson et al., 2015).

In the counterfactual analysis relatively little of the variation in the center-of-gravity in either season or size-class could be attributed to the covariates (Fig. 7). This was true whether the model was fit with or without NEAMAP data (Figs S12 & S13). The observed pattern of a northeastward shift in center-of-gravity was not well captured by the model without the GMRFs, suggesting that the covariates alone are unable to capture this trend, and the majority of the variability of center-of-gravity is driven by unidentified sources.

The proportion of biomass in each area and season is shown in Fig. 8. In both seasons the majority of the recruit biomass is found in the southern area, and recruit biomass has trended downward alongside shelf-wide recruit biomass. In recent years the proportion of recruits in the south has declined while the proportion in the middle area has increased. Spawner biomass is more evenly split between the middle and south regions, but similar to recruits, the proportion of spawner biomass in the south has declined as the proportion of biomass in the middle and north has increased.

4. Discussion

Our results support previous studies that suggest summer flounder are shifting northeast over time. We find this shift in recruits and spawners, and in both seasons. This result holds regardless of whether NEAMAP data are included in the model, and similarly whether a design-based estimator is used instead of the VAST model. The distribution shift is accompanied by a general decreasing trend in biomass in the south of both recruits and spawners.

In contrast to previous studies (Bell et al., 2014, 2015), the distribution shift does not appear to be driven by an increase in the abundance of larger fish, which tend to inhabit more northeastern waters. This is evidenced by the northward shift in small fish (<30cm total length, i.e., recruits). In fact, recruits appear to be shifting northward faster than spawners, suggesting they are not merely tracking spawners northward. The northward shift of recruits also suggests that the driver is unlikely to be spatial patterns of fishing, as recruits are relatively lightly exploited by the fishery. We also find that the distribution shift could not be attributed to either total biomass or environmental covariates. Instead most of the distribution shift is attributed to unidentified sources. The inability of distribution shifts to be attributed to environmental covariates was also found for a west coast groundfish (Thorson et al., 2017), and future work should build on previous studies (e.g., Hodges and Reich, 2010) to better understand when distribution shifts can be attributed to covariates in spatial random effects models. We also recommend further development of methods for incorporating regional covariates into spatial models (e.g., Bacheler et al., 2012; Bartolino et al., 2011).

There are several possible explanations for the inability to identify the driving variable(s) of summer flounder distribution. One is that the model was unable to capture the effect of the driving covariate due to insufficient model flexibility. This could be tested by allowing for a more flexible functional form of the covariate effect, perhaps through the use of splines, although this was outside the scope of our study. However, we urge caution when considering more flexible model structures as spurious relationships can be mistaken as meaningful (Fourcade et al., 2018). An alternative explanation is that the true driving variables were not included in our analysis. This could be tested by including additional covariates. However, the choice of covariates should be selected carefully to reduce the risk of mistakenly identifying a covariate as important simply due to chance (i.e., the multiple testing problem).

Given that the covariates in this analysis were unable to account for a significant proportion of the variability in summer flounder distribution, we caution against using them to generate projections of the future distribution of summer flounder. In general, we suggest that before projecting a species distribution, one should first determine whether the hypothesized driving variables account for a meaningful proportion of the past variability in distribution.

A further extension of the VAST model would be to estimate a seasonal effect within the model, allowing for data from both seasons to be combined into a single model, potentially reducing parameter uncertainty. This functionality is currently under development in VAST, and future work could evaluate its accuracy through simulation tests, as well as its impact on case studies. It could be especially useful for species on the NE Shelf where bi-annual surveys have been carried out for decades.

Acknowledgements

We thank the 2018 summer flounder stock assessment working group for helpful feedback on an earlier draft of this manuscript. We also thank James Gartland for assistance with the NEAMAP data set.

References

Adams, C.F., Alade, L.A., Legault, C.M., O'Brien, L., Palmer, M.C., Sosebee, K.A., Traver, M.L., 2018. Relative importance of population size, fishing pressure and temperature on the spatial distribution of nine Northwest Atlantic groundfish stocks. PLOS ONE 13, e0196583. https://doi.org/10.1371/journal.pone.0196583

Azarovitz, T., 1981. A brief historical review of the Woods Hole Laboratory trawl survey time series, in: Canadian Special Publications of Fisheries and Aquatic Sciences. pp. 62–67.

Bacheler, N.M., Ciannelli, L., Bailey, K.M., Bartolino, V., 2012. Do walleye pollock exhibit flexibility in where or when they spawn based on variability in water temperature? Deep Sea Res. Part II Top. Stud. Oceanogr., Understanding Ecosystem Processes in the Eastern Bering Sea 65–70, 208–216. https://doi.org/10.1016/j.dsr2.2012.02.001

Bartolino, V., Ciannelli, L., Bacheler, N.M., Chan, K.-S., 2011. Ontogenetic and sex-specific differences in density-dependent habitat selection of a marine fish population. Ecology 92, 189–200. https://doi.org/10.1890/09-1129.1

Bell, R.J., Hare, J.A., Manderson, J.P., Richardson, D.E., 2014. Externally driven changes in the abundance of summer and winter flounder. ICES J. Mar. Sci. 71, 2416–2428. https://doi.org/10.1093/icesjms/fsu069

Bell, R.J., Richardson, D.E., Hare, J.A., Lynch, P.D., Fratantoni, P.S., 2015. Disentangling the effects of climate, abundance, and size on the distribution of marine fish: an example based on four stocks from the Northeast US shelf. ICES J. Mar. Sci. 72, 1311–1322. https://doi.org/10.1093/icesjms/fsu217

Fourcade, Y., Besnard, A.G., Secondi, J., 2018. Paintings predict the distribution of species, or the challenge of selecting environmental predictors and evaluation statistics. Glob. Ecol. Biogeogr. 27, 245–256. https://doi.org/10.1111/geb.12684

Friedland, K.D., McManus, M.C., Morse, R.E., Link, J.S., In press. Event scale and persistent drivers of fish and macroinvertebrate distributions on the Northeast US Shelf. ICES J. Mar. Sci. https://doi.org/10.1093/icesjms/fsy167

Henderson, M.E., Mills, K.E., Thomas, A.C., Pershing, A.J., Nye, J.A., 2017. Effects of spring onset and summer duration on fish species distribution and biomass along the Northeast United States continental shelf. Rev. Fish Biol. Fish. 27, 411–424. https://doi.org/10.1007/s11160-017-9487-9

Hodges, J.S., Reich, B.J., 2010. Adding Spatially-Correlated Errors Can Mess Up the Fixed Effect You Love. Am. Stat. 64, 325–334. https://doi.org/10.1198/tast.2010.10052

Kleisner, K.M., Fogarty, M.J., McGee, S., Hare, J.A., Moret, S., Perretti, C.T., Saba, V.S., 2017. Marine species distribution shifts on the U.S. Northeast Continental Shelf under continued ocean warming. Prog. Oceanogr. 153, 24–36. https://doi.org/10.1016/j.pocean.2017.04.001

Kristensen, K., Nielsen, A., Berg, C.W., Skaug, H., Bell, B.M., 2016. TMB: Automatic differentiation and laplace approximation. J. Stat. Softw. 70, 1–21.

Miller, T.J., 2013. A comparison of hierarchical models for relative catch efficiency based on paired-gear data for US Northwest Atlantic fish stocks. Can. J. Fish. Aquat. Sci. 70, 1306–1316. https://doi.org/10.1139/cjfas-2013-0136

Miller, T.J., Das, C., Politis, P.J., Miller, A.S., Lucey, S.M., Legault, C.M., Brown, R.W., Rago, P.J., 2010. Estimation of Albatross IV to Henry B. Bigelow Calibration Factors (Northeast Fisheries Science Center Reference Document No. 10– 05). U.S. Department of Commerce, Woods Hole, MA.

NEFSC, In Review. 66th Northeast Regional Stock Assessment Workshop (66th SAW) Assessment Report., Northeast Fisheries Science Center Reference Document. Department of Commerce, Woods Hole, Ma.

Nye, J.A., Link, J.S., Hare, J.A., Overholtz, W.J., 2009. Changing spatial distribution of fish stocks in relation to climate and population size on the Northeast United States continental shelf. Mar. Ecol. Prog. Ser. 393, 111–129.

Pearl, J., 2009. Causal inference in statistics: An overview. Stat. Surv. 3, 96–146. https://doi.org/10.1214/09-SS057

Perry, A.L., Low, P.J., Ellis, J.R., Reynolds, J.D., 2005. Climate Change and Distribution Shifts in Marine Fishes. Science 308, 1912–1915. https://doi.org/10.1126/science.1111322

Pinsky, M.L., Fogarty, M., 2012. Lagged social-ecological responses to climate and range shifts in fisheries. Clim. Change 115, 883–891. https://doi.org/10.1007/s10584-012-0599-x

Pinsky, M.L., Worm, B., Fogarty, M.J., Sarmiento, J.L., Levin, S.A., 2013. Marine Taxa Track Local Climate Velocities. Science 341, 1239–1242. https://doi.org/10.1126/science.1239352

Sackett, D.K., Able, K.W., Grothues, T.M., 2007. Dynamics of summer flounder, Paralichthys dentatus, seasonal migrations based on ultrasonic telemetry. Estuar. Coast. Shelf Sci. 74, 119–130. https://doi.org/10.1016/j.ecss.2007.03.027

Smith, T.D., 2002. The Woods Hole bottom-trawl resource survey: development of fisheries-independent multispecies monitoring. ICES Mar. Sci. Symp. 215, 474–482.

Terceiro, M., 2001. The summer flounder chronicles: Science, politics, and litigation, 1975–2000. Rev. Fish Biol. Fish. 11, 125–168. https://doi.org/10.1023/A:1015260005887

Thorson, J.T., Barnett, L.A.K., 2017. Comparing estimates of abundance trends and distribution shifts using single- and multispecies models of fishes and biogenic habitat. ICES J. Mar. Sci. 74, 1311–1321. https://doi.org/10.1093/icesjms/fsw193

Thorson, J.T., Ianelli, J.N., Kotwicki, S., 2017. The relative influence of temperature and size-structure on fish distribution shifts: A case-study on Walleye pollock in the Bering Sea. Fish Fish. 18, 1073–1084. https://doi.org/10.1111/faf.12225

Thorson, J.T., Shelton, A.O., Ward, E.J., Skaug, H.J., 2015. Geostatistical delta-generalized linear mixed models improve precision for estimated abundance indices for West Coast groundfishes. ICES J. Mar. Sci. 72, 1297–1310. https://doi.org/10.1093/icesjms/fsu243

Wigley, S.E., McBride, H.M., McHugh, N.J., 2003. Length-weight relationships for 74 fish species collected during NEFSC research vessel bottom trawl surveys, 1992-99 (NOAA Technical Memorandum No. 171). National Marine Fisheries Service.

Woillez, M., Poulard, J.-C., Rivoirard, J., Petitgas, P., Bez, N., 2007. Indices for capturing spatial patterns and their evolution in time, with application to European hake (Merluccius merluccius) in the Bay of Biscay. ICES J. Mar. Sci. 64, 537–550. https://doi.org/10.1093/icesjms/fsm025

Figures

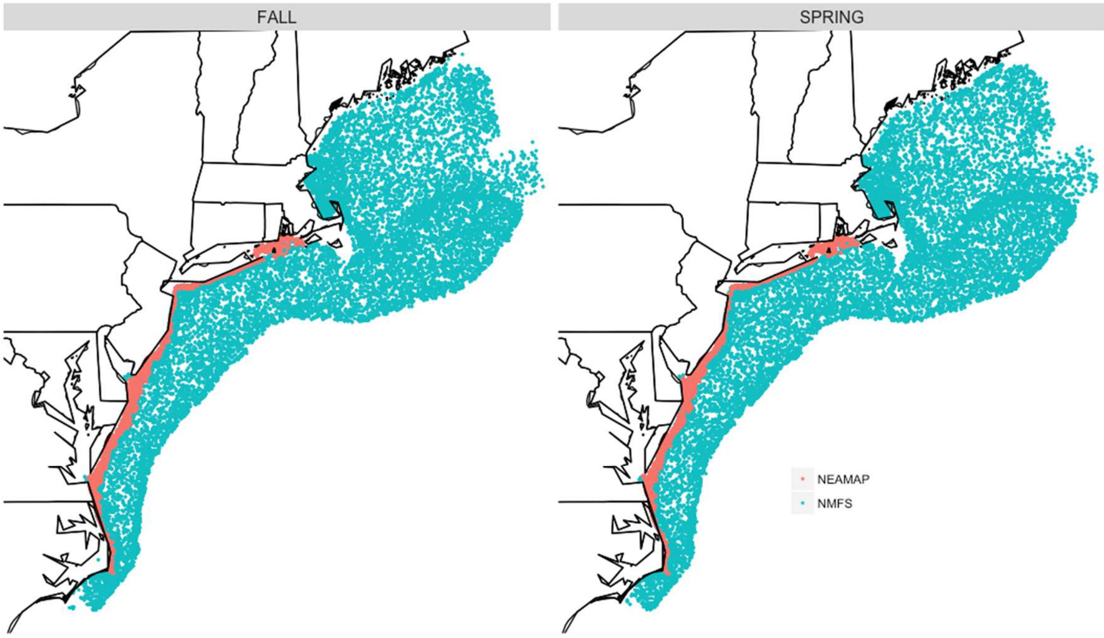

Figure 1. Tow locations for the NEAMAP (2007 – 2016) and NMFS (1976 – 2016) surveys in each season.

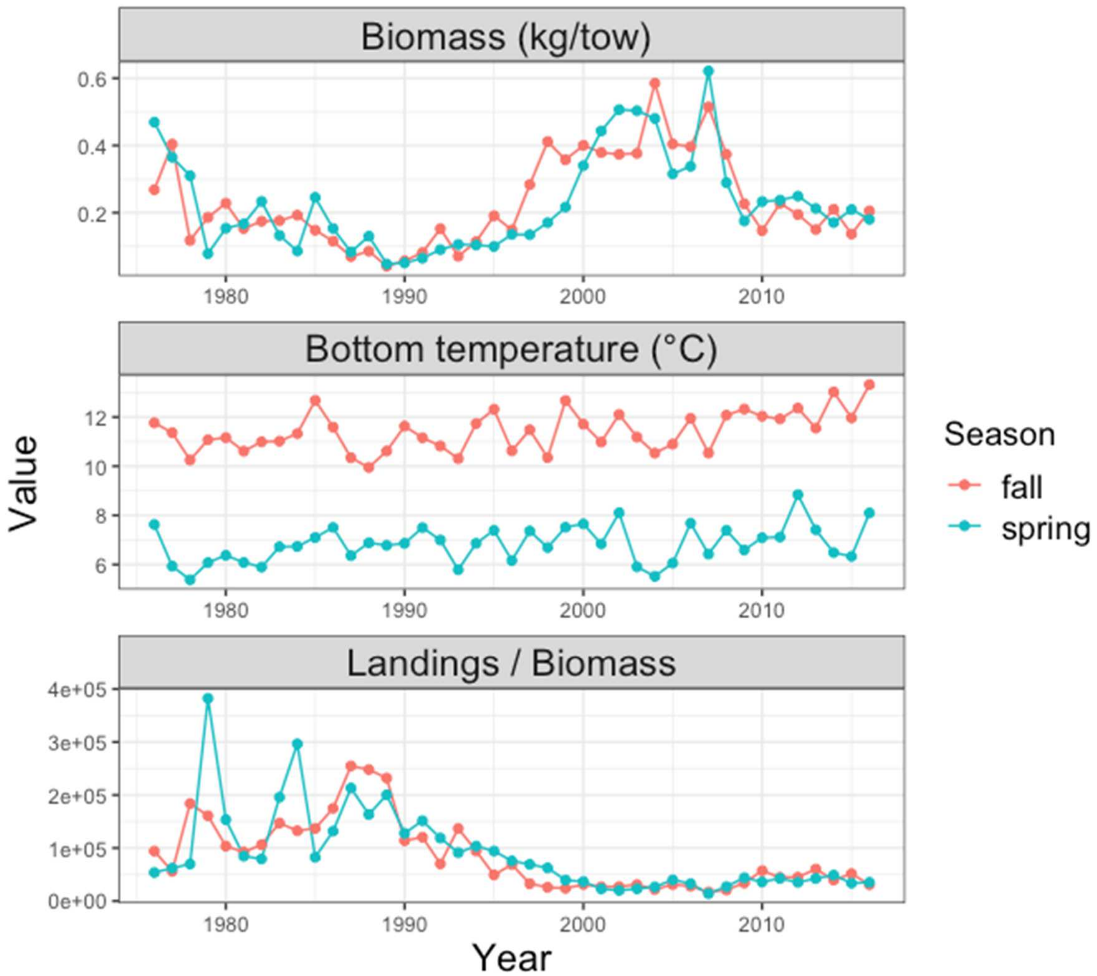

Figure 2. Time series of regional covariates.

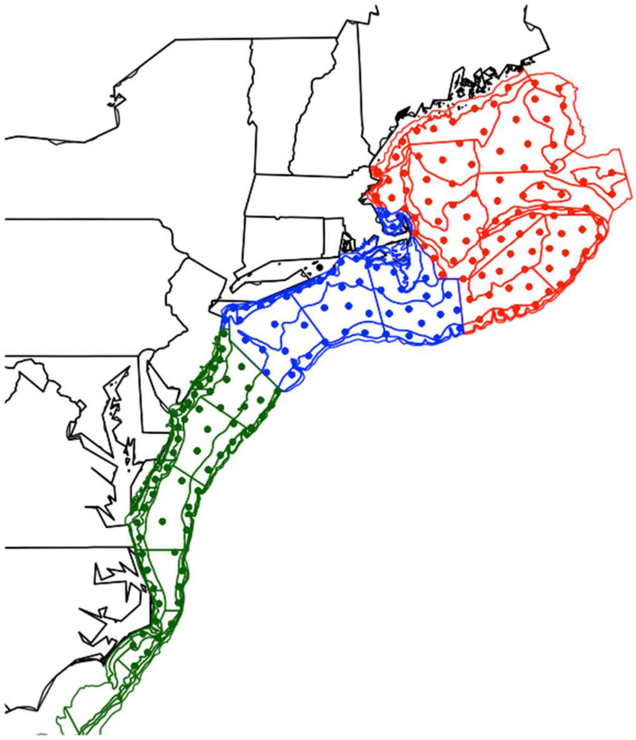

Figure 3. Division of NMFS survey strata into subareas for analysis of biomass trends in each area. The shelf is divided into north (red), middle (blue) and south (green). Knots associated with each area are shown in the same color.

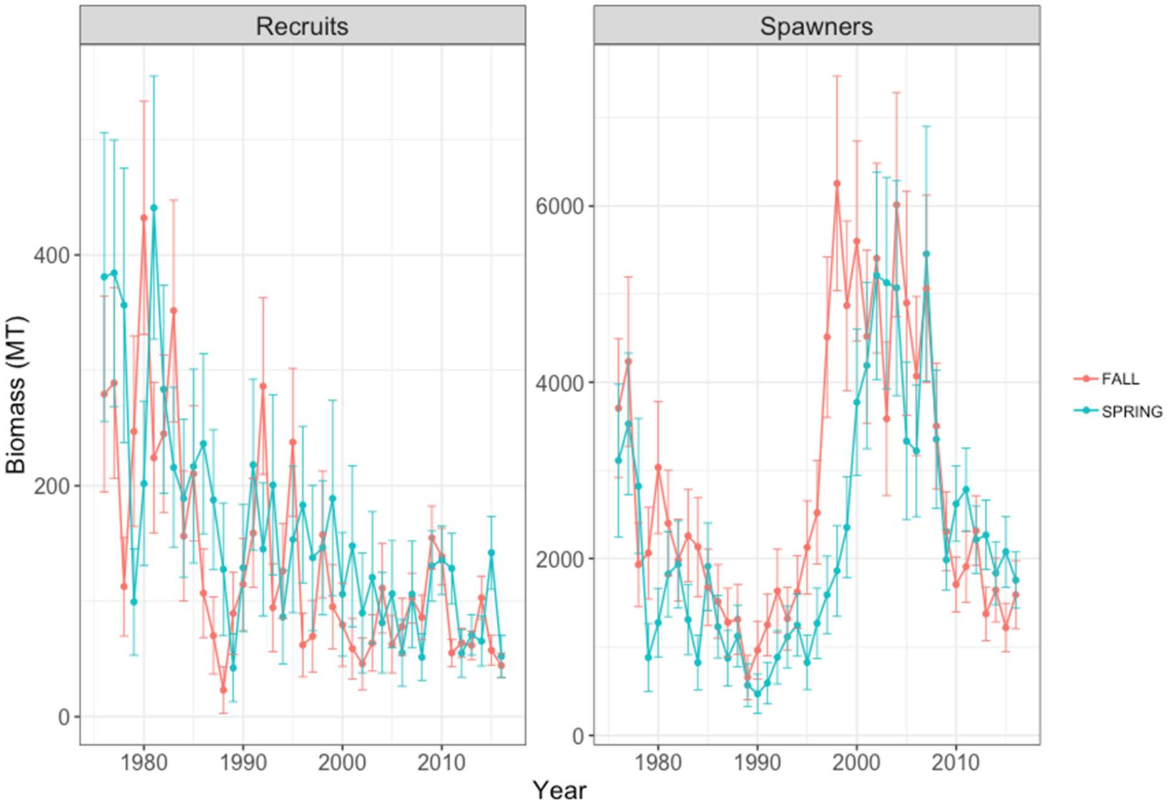

Figure 4. Biomass time series generated by VAST for each season. Error bars are 95% confidence intervals.

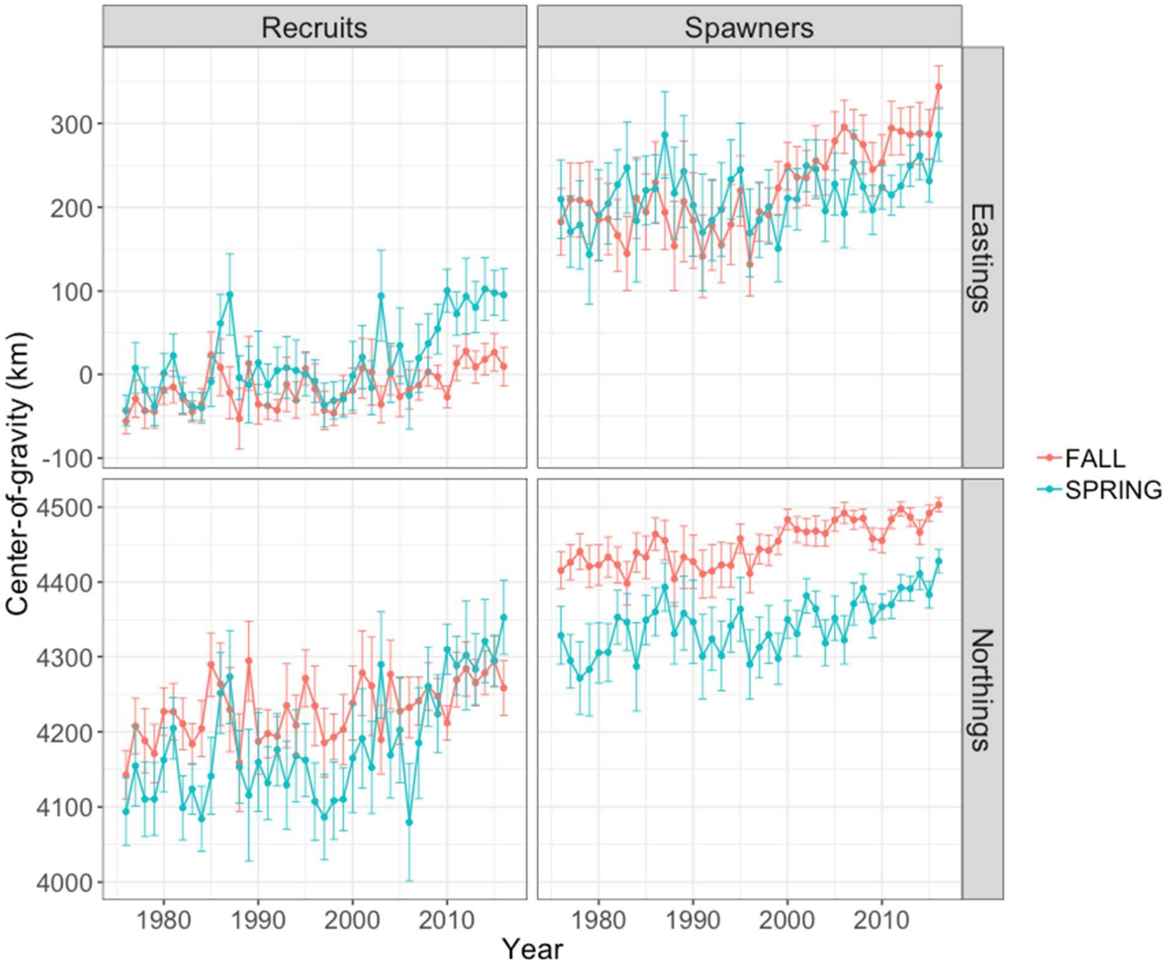

Figure 5. Center-of-gravity for each season and size category. Error bars are the 95% confidence intervals.

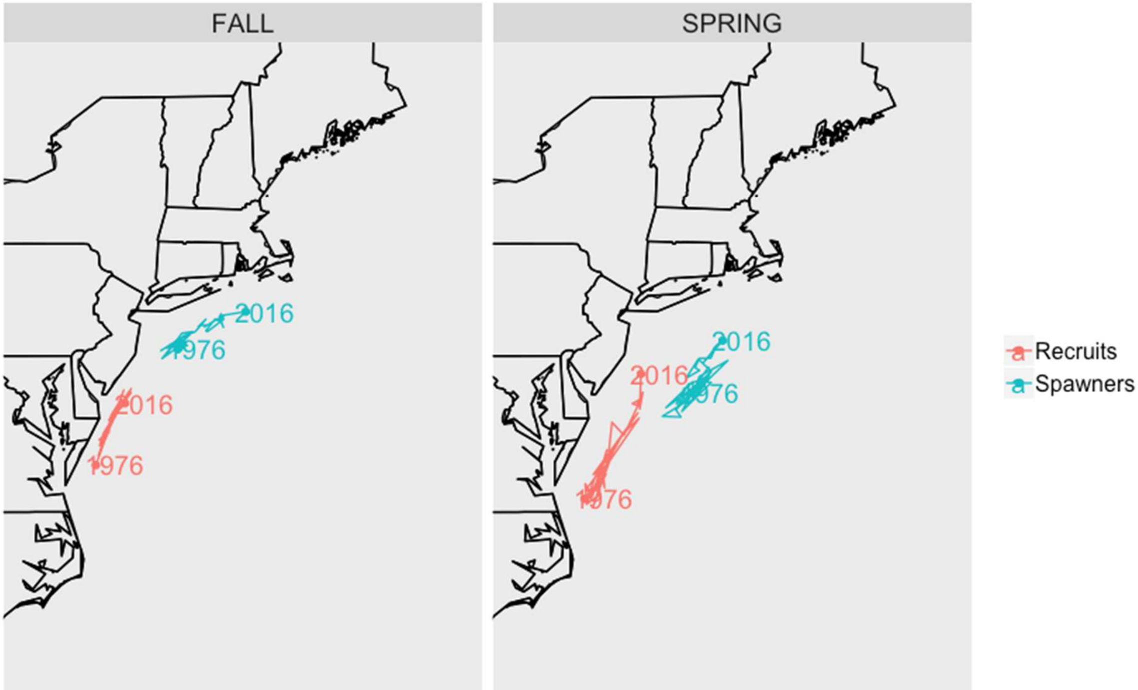

Figure 6. Map of the center-of-gravity in each season for each size category.

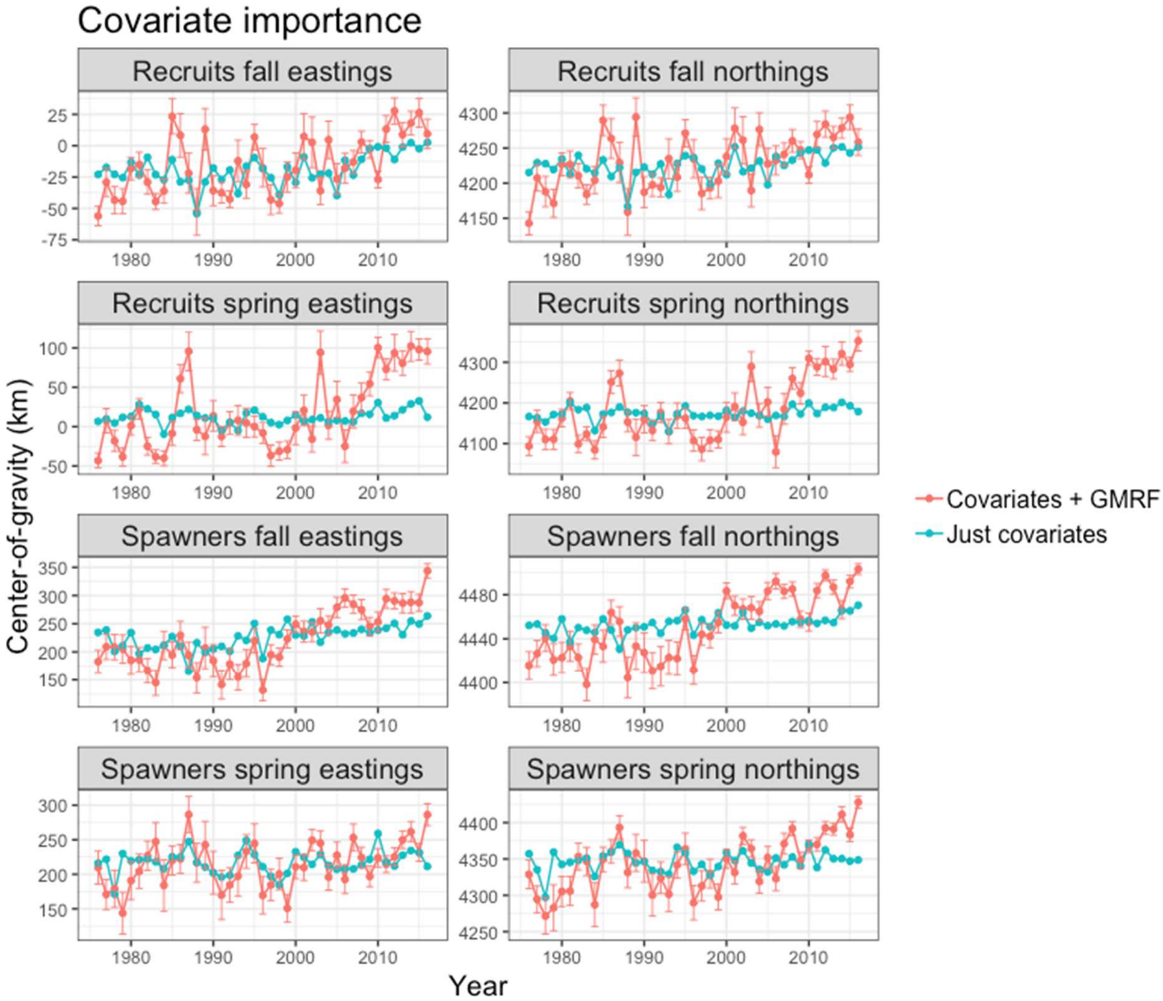

Figure 7. Counterfactual plots showing the ability of covariates to account for variability in the center-of-gravity in each season.

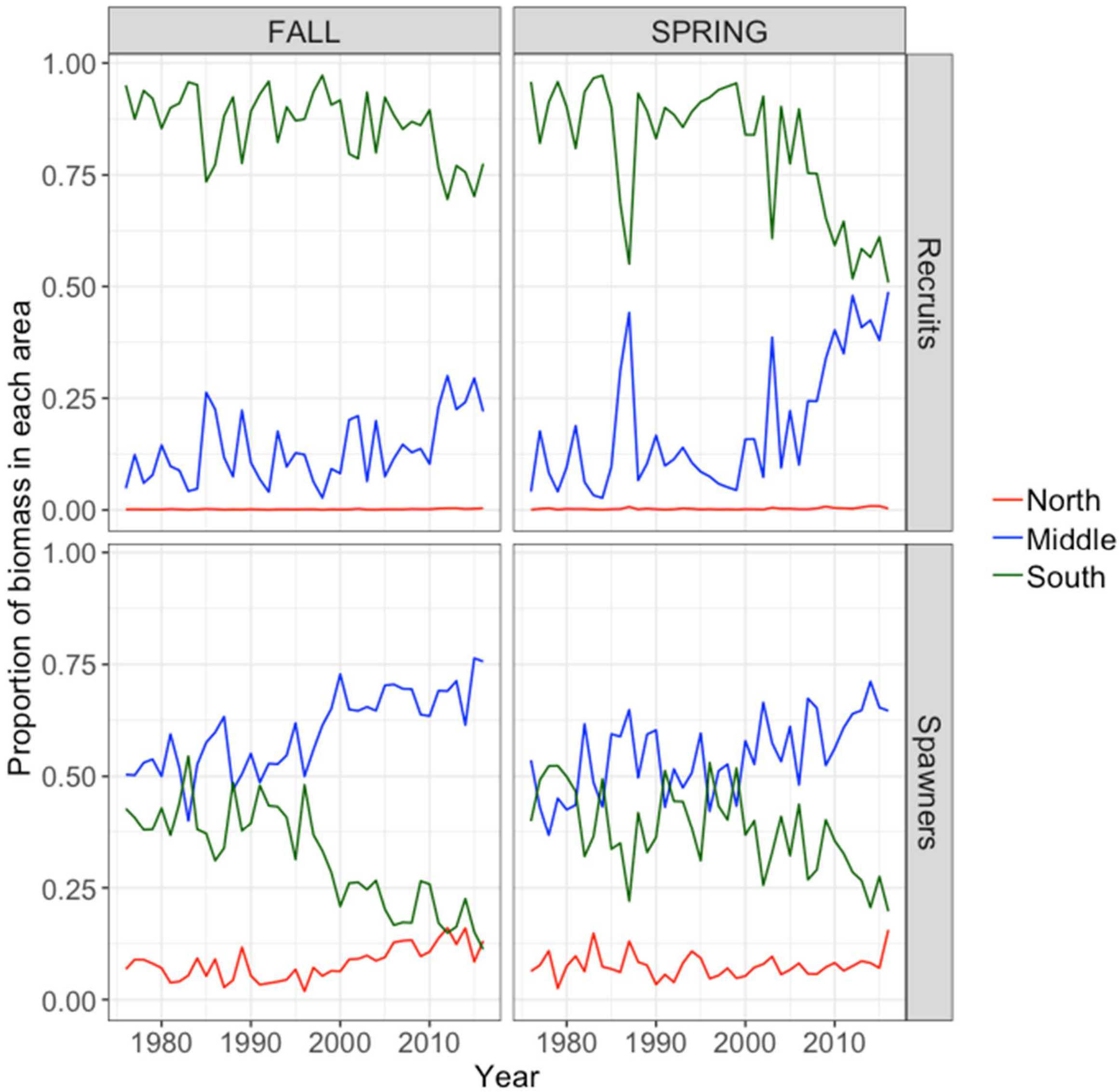

Figure 8. Proportion of biomass in each subarea.